JOURNAL OF MODERN OPTICS
2021, VOL. 68, NO. 15, 784–791
https://doi.org/10.1080/09500340.2021.1947533

Taylor & Francis
Taylor & Francis Group



# Circular anti-resonance fibre supporting orbital angular momentum modes with flat dispersion, high purity and low confinement loss

Haihao Fu[a], Zao Yi[b], Ying Shi[a], Chao Liu[a], Jingwei Lv[a], Lin Yang[a] and Paul K. Chu[c]

[a]School of Physics and Electronic Engineering, Northeast Petroleum University, Daqing, People's Republic of China; [b]Joint Laboratory for Extreme Conditions Matter Properties, Southwest University of Science and Technology, Mianyang, People's Republic of China; [c]Department of Physics, Department of Materials Science and Engineering, and Department of Biomedical Engineering, City University of Hong Kong, Kowloon, Hong Kong, People's Republic of China

**ABSTRACT**

A novel ring anti-resonance fibre (ARF) is designed and demonstrated for the transmission of orbital angular momentum (OAM) modes. The fibre consists of two layers of negative curvature tubes arranged orderly inside and outside the ring region and OAM modes can be transmitted in the ring region. The properties of the fibre are investigated by the finite element method based on the COMSOL multiphysics software and a manufacturing method is proposed. The fibre shows stable transmission of 30 OAMs in the 1.5–1.6 $\mu$m band, low and flat dispersion (5.98 ps/(km nm)), extremely small nonlinear coefficient (0.539 $km^{-1}$ $W^{-1}$ at 1.55 $\mu$m) and confinement loss ($10^{-9}$–$10^{-11}$ dB/m), as well as high OAM purity (larger than 98.295%). Therefore, the structure has immense potential in optical communication.

**ARTICLE HISTORY**
Received 18 May 2021
Accepted 18 June 2021

**KEYWORDS**
Orbital angular momentum; anti-resonance fibre; chromatic dispersion; confinement loss

## 1. Introduction

Space division multiplexing (SDM) and mode division multiplexing (MDM) are two effective techniques to expand capacity of optical communication systems [1–3]. As another form of MDM, optical orbital angular momentum (OAM) has become a research hotspot in optical fibre communication because it can realize large capacity stable transmission theoretically due to infinite orthogonal basis [4,5]. At present, the step index fibre (SIF) [6], graded index fibre (GIF) [7] and photonic crystal fibre (PCF) [8] can transmit optical OAM stably. In particular, PCF has become the main medium for optical orbital angular momentum transmission because of the flexible structural design and good compatibility. However, one of the impediments for OAM in PCF is the easy occurrence of mode coupling, thereby making the effective index difference to be less than $1 \times 10^{-4}$ and difficult for OAM modes to propagate stably [9]. In addition, although PCFs deliver excellent performance by rational design of cladding air holes, it is still difficult to minimize scattering loss and absorption loss [10], which can affect production and application negatively. Consequently, there have been efforts to design optical fibres with low loss and flat dispersion to improve the quality of OAM mode transmission in optical fibres.

In the anti-resonance effect [11], when light is coupled with the core and transmitted to the interface between the core and cladding, the light satisfying the resonance condition is transmitted through the cladding, while light not satisfying the resonance condition is reflected back to the core region and continue to propagate forward. The anti-resonance fibre (ARF) has a negative curvature and the cladding is composed of a circular or elliptical tubes [12]. The surface normal vector at the core boundary is opposite to the radial unit vector and the negative curvature can suppress mode degeneracy [13] to facilitate OAM mode transmission. Moreover, the limitation of scattering loss and absorption loss at short and long wavelengths can be circumvented by adopting the special guiding principle of ARF to reduce the loss of the fibre. For example, Kosolapov et al. [14] proposed an ARF with double capillaries and single rings with the same wall thickness showing a loss at 1.85 $\mu$m wavelength of not higher than 75 dB/km. Chaudhuri et al. [15] illustrated a negative curvature ARF with nested elliptic cladding tubes for ultra-low loss transmission at 1.55 $\mu$m. Hayes [16] et al. designed a hollow core ARF composed of

**CONTACT** Chao Liu msm-liu@126.com School of Physics and Electronic Engineering, Northeast Petroleum University, Daqing 163318, People's Republic of China

seven single ring cladding tubes with a minimum loss of 25 dB/km at 1.2 $\mu$m and recently, Chen Xiang et al. [17] proposed a negative curvature ARF with loss of less than 1 dB/km and excellent single-mode performance.

In this work, a circular ARF is designed for the transmission of 30 OAM modes in the range of 1.50 $\mu$m to 1.60 $\mu$m and the effective index difference of all the modes are larger than $10^{-4}$. Our analysis conducted with COMSOL Multiphysics reveals flat dispersion, low confinement loss, large effective mode area and high OAM purity. The influence of the wall thickness of the negative curvature anti-resonance tube on the dispersion flatness and OAM purity is assessed and the manufacturing process for the fibre structure is proposed.

## 2. ARF design and numerical simulation

The cross-section of the ARF which can propagate OAM modes with the negative curvature anti-resonance tube is shown in Figure 1. In the finite element method (FEM), the free triangular mesh with the minimum element of 0.012 μm is adopted and the degree of freedom is 380,253. The geometry has 117 domains, 460 boundaries and 394 vertices. A layer containing the negative curvature anti-resonance tubes with the same wall thickness and tangent to the annular region is laid inside and outside the annular region, respectively. The inner tubes are dense and evenly distributed inside the annular region. Eighteen anti-resonance tubes with a large inner radius, which effectively limit the light that does not meet the resonance condition in the ring region, are placed outside the annular area to reduce dispersion and mode degeneracy.

The cladding is air except the wall of the anti-resonance tube to increase the effective index difference and transmission of more OAM modes. $R_0 = 9\ \mu$m is the inner radius of the annular region, $l_0 = 3.5\ \mu$m is the thickness of the annular region, $r_1 = 2\ \mu$m and $r_2 = 0.8\ \mu$m are the inner radius of two kinds of negative curvature tubes respectively, $t = 0.5\ \mu$m is the wall thickness, and $R_1 = 17\ \mu$m is the radius of cladding. The effect of $l_0$ on the performance of the optical fibre from 2 $\mu$m to 4 $\mu$m is considered when designing the structure. The simulation results demonstrate that a larger $l_0$ produces smaller dispersion and confinement loss. However, the number of OAM modes begins to decrease when $l_0$ is greater than 3.5 $\mu$m and the ring region thickness is thus set to be 3.5 $\mu$m. In Figure 1, the indigo area is the perfect matching layer (PML) and the blue region is $SiO_2$, whose refractive index is determined by Sellmeier equation [18] as shown in Equation (1):

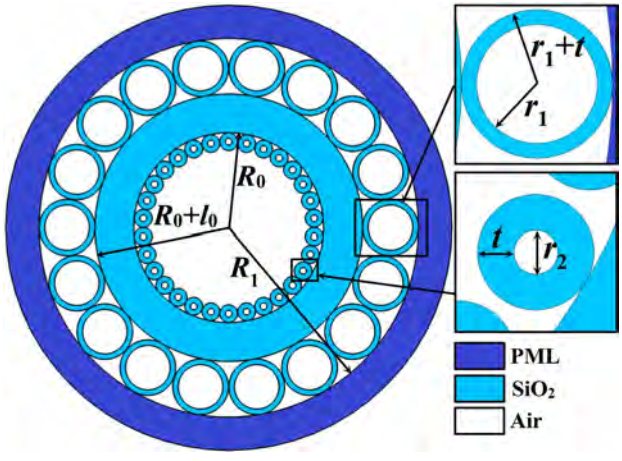


**Figure 1.** Cross-section of the annular structure in the ARF.

$$n^2(\lambda) = 1 + \frac{A_1\lambda^2}{\lambda^2 - B_1} + \frac{A_2\lambda^2}{\lambda^2 - B_2} + \frac{A_3\lambda^2}{\lambda^2 - B_3} \quad (1)$$

where $A_1 = 0.6961663$, $A_2 = 0.4079426$, $A_3 = 0.897479$, $B_1 = 0.0684043$, $B_2 = 0.1162414$ and $B_3 = 9.896161$. After calculating the original data with COMSOL, various optical properties can be obtained using MATLAB.

## 3. Results and discussion

To determine the properties of the ARF and transmission of OAM modes, the effective refractive index, effective refractive index difference, dispersion, effective mode field area, nonlinear coefficient, limiting loss and numerical aperture are derived. The influence of the negative curvature tube wall thickness on dispersion and confinement loss is also evaluated.

### 3.1. Transmission modes

The vortex beam has a helical phase $\exp(\pm il\theta)$, where $l$ is the number of topological charges and $\theta$ is the azimuth angle. As a new dimension of optical communication, OAM can be defined as the superposition of odd and even modes of the same order vector mode. OAM mode is widely used in optical communication because of its infinite number of orthogonal bases. In the fibre, $HE_{l+1,m}$ and $EH_{l-1,m}$ are the eigenmodes of $OAM_{l,m}$ where $m$ is the number of concentric rings in the intensity distribution and equal to 1. The OAM mode in the optical fibre is composed of the intrinsic mode [19]:

$$\boldsymbol{OAM}^{\pm}_{\pm l,m} = \boldsymbol{HE}^{even}_{l+1,m} \pm i\boldsymbol{HE}^{odd}_{l+1,m} \quad \text{and}$$
$$\boldsymbol{OAM}^{\mp}_{\pm l,m} = \boldsymbol{EH}^{even}_{l-1,m} \pm i\boldsymbol{EH}^{odd}_{l-1,m} \quad (2)$$

where '±' or '∓' is the circular polarization direction and '+' and '−' denote the right-handed and left-handed circular polarization, respectively. Equation (2) shows that $OAM_{1,m}$ composed of odd and even modes of $HE_{2,1}$ with

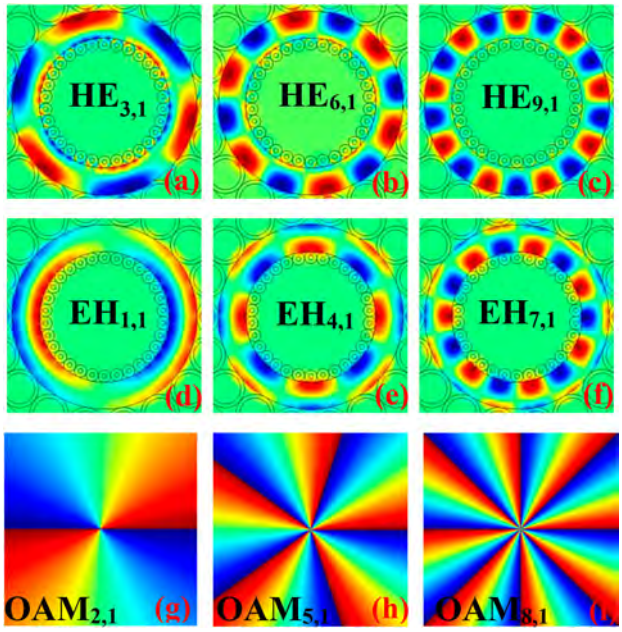


**Figure 2.** (a)–(f) Optical field distributions of the partial HE and EH modes in the *z* direction at 1.55 $\mu$m; (g)–(i) Phase diagrams of the partially displayed OAM modes.

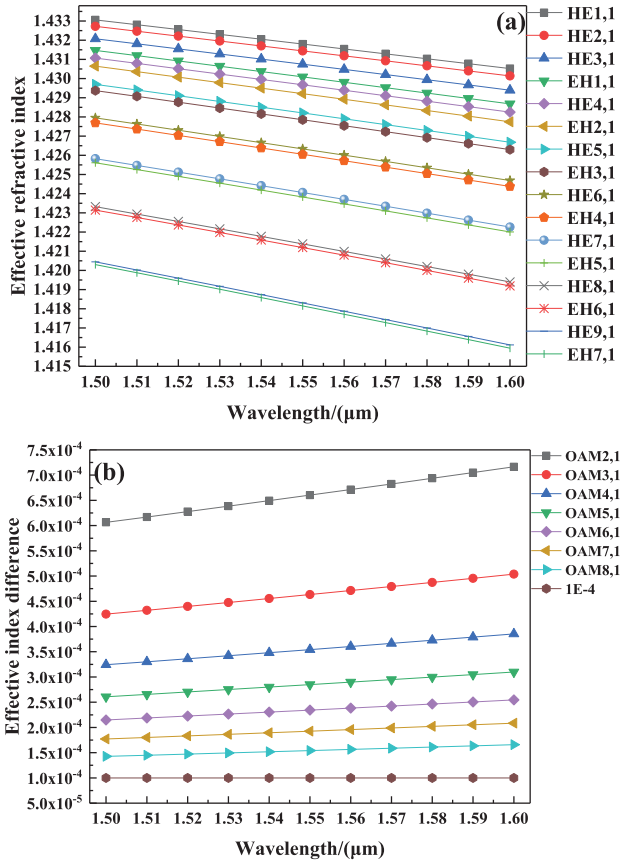


**Figure 3.** (a) Effective mode index of all the modes and (b) Effective refractive index of the OAM modes.

the same polarization and rotation direction of the wave front has two modes. The OAM patterns with the same topological load $l$ and $m$ belong to the same OAM pattern group. $\mathrm{OAM}_{l,m}$ has two degeneracies when $l = 1$ and four degeneracies when $l > 1$. Therefore, the fibre has 30 OAM modes including OAM± ±1,1$\mathrm{HE}_{2,1}$,OAM± ±$l$,1$\mathrm{HE}_{l+1,1}$,$\mathrm{EH}_{l-1,1}$ ($l$ = 2–8). Figure 2(a–f) shows the field distributions in the $z$ direction for partial modes at 1.55 $\mu$m. The OAM modes of the EH modes are more stable than those of HE under an external influence because the EH modes are closer to the fibre core than the HE modes. Figure 2(g–i) shows the phase distributions of the OAM modes which change $\pi/2$ azimuthally and therefore, these modes can be de-multiplexed with conjugating phase modes.

### 3.2. Effective refractive index

The real part and imaginary parts of the effective mode index determine the dispersion and confinement loss and it is the basic physical quantity of the ARF. Figure 3(a) exhibits the effective index of all the OAM modes and stable transmission of the OAM mode in the optical fibre depends on the effective index difference. It has been demonstrated that the effective index difference between the HE and EH modes which can synthesize the same order OAM should be greater than $1 \times 10^{-4}$ [20,21], otherwise the OAM modes will become degenerate and form LP modes during transmission in the fibre, which is not conducive to optical communication. The variation of the effective mode refractive index difference with wavelength is shown in Figure 3(b).

The longer the wavelength, the smaller is the effective refractive index. Moreover, the effective mode index is inversely proportional to the wavelength and the effective refractive index difference is proportional to the wavelength. The OAM mode with the smallest effective index difference is $\mathrm{OAM}_{8,1}$ at 1.50 $\mu$m, which is $1.426 \times 10^{-4}$, and the refractive index difference of all the modes is greater than $1.541 \times 10^{-4}$ at 1.55 $\mu$m. Consequently, mode degeneracy does not occur in the advanced ARF.

### 3.3. Chromatic dispersion

Pulse broadening produces signal distortion when different components of the optical signal propagate at different speeds for a certain distance in the optical fibre and it is called dispersion. The transmission distance of the optical signal decreases and the confinement loss increases when dispersion is too large and hence, dispersion in the structure should be as small and flat as possible. The dispersion of ARF is expressed by

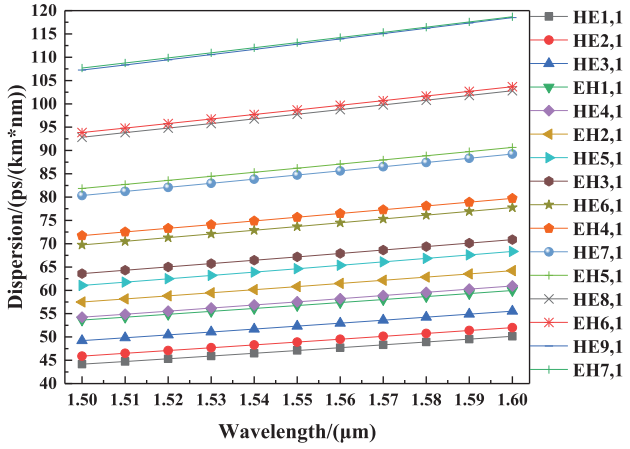


**Figure 4.** Chromatic dispersion of the HE and EH modes in the advanced fibre.

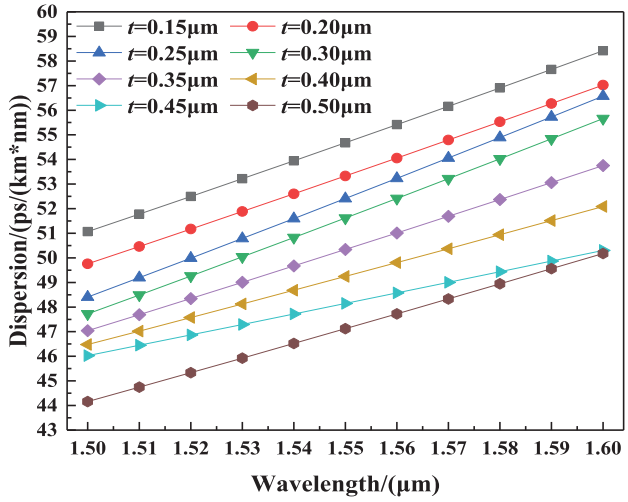


**Figure 5.** Relationship between dispersion and wall thickness of $HE_{1,1}$.

Equation (3) [22]:

$$D = -\frac{\lambda}{c}\frac{d^2 Re(n_{\text{eff}})}{d\lambda^2} \tag{3}$$

where $c = 3\times10^8$ m/s is the speed of light, λ is the wavelength and $Re(n_{\text{eff}})$ is the real part of the effective refractive index.

Dispersion of the HE and EH modes (Figure 4) increases with increasing wavelength and that of higher-order modes is larger than that of lower order modes because the refractive index variation of higher-order modes is greater than that of the lower mode as the wavelength goes up. The EH mode of the same order of OAM is closer to the core and the HE mode is near the cladding for the same wavelength. The EH mode has a longer transmission distance and larger pulse width when it propagates to the cladding leading to higher dispersion. The mode with minimum dispersion is $HE_{1,1}$ and as low as 44.158 ps/(km nm) at 1.50 $\mu$m, while the smallest variation is 5.98 ps/(km nm) for $HE_{1,1}$. Concurrently, the mode with maximal dispersion is $EH_{7,1}$ and 118.688 ps/(km nm) at 1.55 $\mu$m, whereas the utmost variation of 10.9923 ps/(km nm) is observed from $EH_{7,1}$. The small and flat dispersion produces the excellent properties in optical fibre communication. The dispersion flatness of the fibre and comparison with other structures are shown in Table 1. The influence of the negative curvature tube wall thickness on dispersion of $HE_{1,1}$ represented in Figure 5 is also investigated at 1.55 $\mu$m. Dispersion increases with increasing wavelength for any wall thickness and that of $HE_{1,1}$ decreases and tends to be flat when the wall thickness becomes larger. In fact, the thicker the negative curvature tube, the smaller is dispersion. However, the number of OAM modes decreases when $t > 0.5\,\mu$m and so the optimal thickness of the negative curvature tube is 0.5 $\mu$m.

### 3.4. Nonlinear coefficient and effective mode area

The region of the light field distribution is called the effective mode area, which reflects the concentration of photon energy in the fibre. The effective mode area is expressed by Equation (4) [23]:

$$A_{eff} = \frac{\left(\iint |E(x,y)|^2 dxdy\right)^2}{\iint |E(x,y)|^4 dxdy} \tag{4}$$

where $E(x,y)$ is the electric vector of the cross-section of the optical fibre during light propagation and can be evaluated by COMSOL directly. Another important physical quantity related to transmission of OAM modes is the nonlinear coefficient which is inversely proportional to the effective mode area as shown by Equation (5) [24]:

$$\gamma = \frac{2\pi n}{\lambda A_{eff}} \tag{5}$$

where $n = 2.3\times10^{-20}\ \text{m}^2\,\text{W}^{-1}$ is the nonlinear refractive index of silica, λ is the wavelength, and $A_{\text{eff}}$ is the effective mode area. The nonlinear coefficient can be utilized to measure the nonlinear effects in the structure. It is

**Table 1.** Comparison of the minimum dispersion flatness.

| This paper | Ref. [27] | Ref. [28] | Ref. [29] | Ref. [30] |
|---|---|---|---|---|
| 5.98 ps/(km·nm) | 32 ps/(km·nm) | 60 ps/(km·nm) | 18.72 ps/(km·nm) | 53.48 ps/(km·nm) |

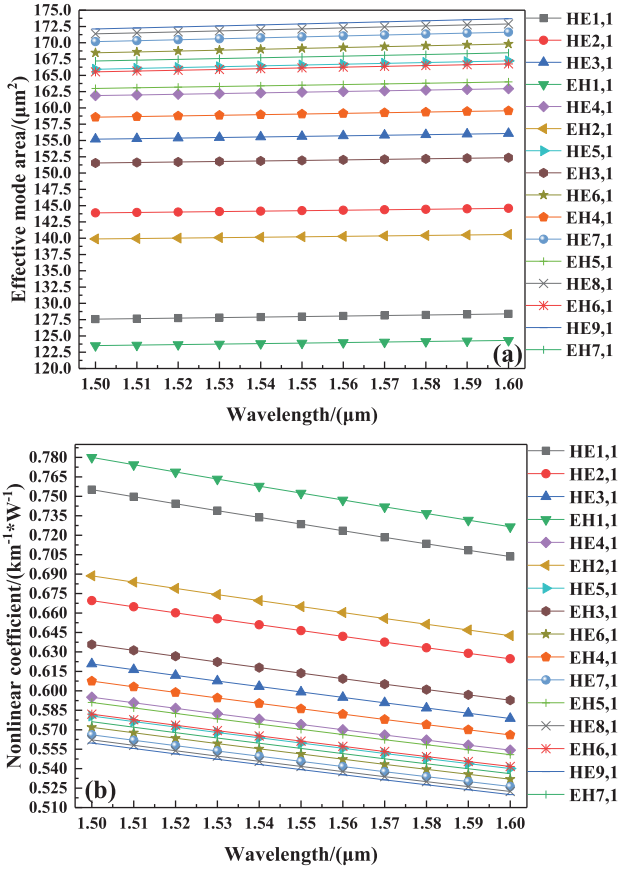


**Figure 6.** (a) Effective mode area and (b) Nonlinear coefficients of the HE and EH modes.

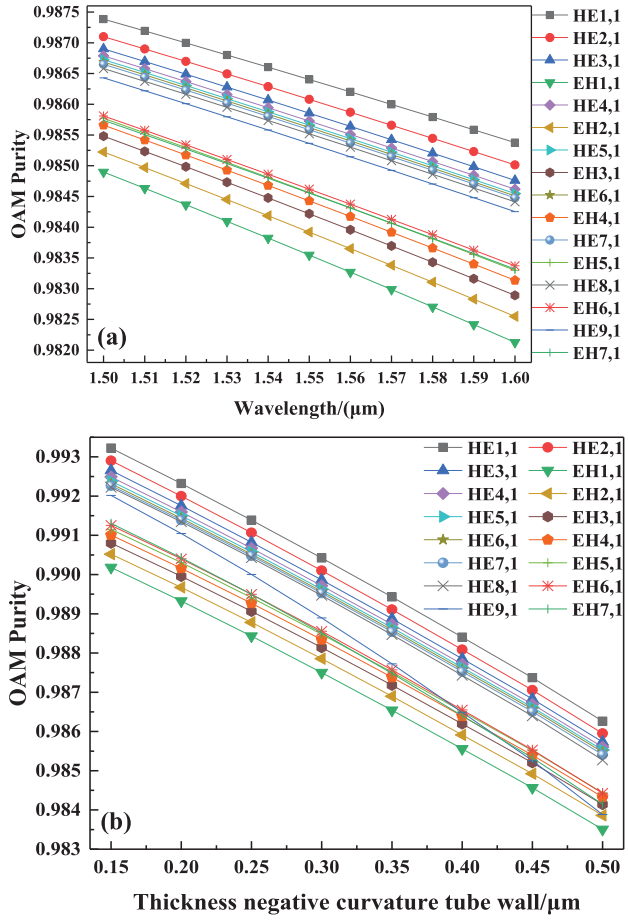


**Figure 7.** (a) Mode purity of the HE and EH modes from 1.50 $\mu$m to 1.60 $\mu$m and (b) variation of the purity of HE and EH modes with the thickness of the negative curvature tube wall at 1.55 $\mu$m

not conducive to the stable transmission of optical signals and actual production of the ARF when the nonlinear coefficient is too large. Therefore, the nonlinear coefficient should be as low as possible. Figure 6(a,b) shows the effective mode area and nonlinear coefficient of the transmitted OAM mode, respectively.

The longer the wavelength, the larger is the mode field area and the smaller the nonlinear coefficient. The reason why the mode order is proportional to the effective mode area is that the circular region has a low ability to limit the higher-order modes, which makes it easy to leak into the cladding. The pattern with the smallest nonlinear coefficient is $HE_{9,1}$ at 1.6 $\mu$m (0.520 $km^{-1}$ $W^{-1}$) and the nonlinear coefficient is as low as 0.539 $km^{-1}$ $W^{-1}$ at 1.55 $\mu$m. The reason for the larger mode area of the HE modes used to synthesize OAM of the same order is that the light field of the HE mode is closer and can leak more easily into the cladding.

### 3.5. OAM purity/mode purity

Mode purity characterizes the mode quality of OAM and the higher the mode purity, the more stable is OAM mode transmission and more complete the signal after de-multiplexing. The purity of the OAM modes can be evaluated qualitatively using the light intensity overlap factor. The mode purity determined by Equation (6) [23] is mainly related to the electric field distribution in the ring region and cross-section of the fibre:

$$\eta = \frac{I_r}{I_c} = \frac{\iint_{\text{ring}} \left|\vec{E}\right|^2 dxdy}{\iint_{\text{cross - section}} \left|\vec{E}\right|^2 dxdy} \tag{6}$$

where $I_r$ and $I_c$ are the light intensity of the ring area and entire fibre section, respectively, which can be computed by COMSOL. Figure 7(a) shows the regulation of wavelength and OAM purity. As shown in Figure 7(a), the mode purity of the HE and EH modes is inversely proportional to the wavelength. All the HE and EH modes propagating in the ARF are more than 98.332% which are high and conducive to optical communication. It is noted that the mode purity of the HE modes is higher than that of the EH modes because the leakage energy of the HE modes is smaller than that of the EH modes. In addition, the variation of the purity of HE and EH modes with

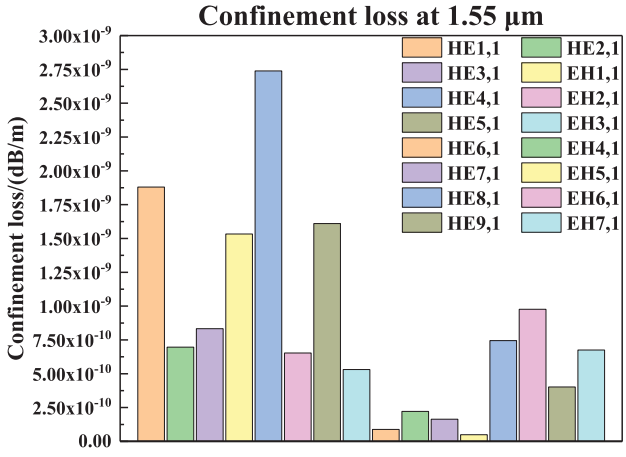


**Figure 8.** Confinement loss of the advanced structure at 1.55 $\mu$m.

thickness of the negative curvature tube wall at 1.55 $\mu$m is determined and displayed in Figure 7(b). As the tube wall becomes thicker, the mode purity of HE and EH modes are decreased And almost all the purity of the mode is still higher than that of EH mode at 1.55 $\mu$m.

### 3.6. Confinement loss

The confinement loss is an important parameter to gauge the performance of optical fibre as it determines the maximum relay distance in the optical communication system and performance of other devices [25]. Owing to the different size and arrangement of the negative curvature tubes, different limiting power to light-wave results in a different loss. The confinement loss can be calculated by Equation (7) [26]:

$$CL = \frac{2\pi}{\lambda}\frac{20}{\ln(10)}10^6 Im(n_{eff}) \tag{7}$$

where $\lambda$ is the wavelength and $Im(n_{\text{eff}})$ is the imaginary part of the effective refractive index which can be calculated by COMSOL. Because ARF can circumvent the limitation of absorption loss and scattering loss, loss is reduced significantly and so the loss is lower than that of most other fibres. Figure 8 shows that the confinement loss at 1.55 $\mu$m.

The confinement loss of all the modes is between $10^{-11}$ and $10^{-9}$ and the minimum value is $8.82 \times 10^{-11}$ dB/m ($HE_{6,1}$) which is very low. It facilitates not only stable transmission of OAM modes but also actual fibre design. The confinement loss of this fibre is compared to that of other structures in Table 2.

### 3.7. Fabrication process

The circular ARF structure described in this paper can be produced by the stack tube technique. A plurality of small radius negative curvature tubes is provided at predetermined peripheral positions inside the annular tube having an inner surface and central longitudinal axis such that the negative curvature tubes are spaced around the inner surface. Each negative curvature tube is in contact with the inner surface, so that the central longitudinal axis of each negative curvature tube is at a negative radial distance from the central longitudinal axis of the annular tube. In the same way, a plurality of large radius negative curvature tubes in contact with the outer surface is provided at a predetermined peripheral position of the outer surface of the annular tube and spaced around the outer surface, so that the central longitudinal axis of each negative curvature tube is at a positive radial distance from the central longitudinal axis of the annular tube. When the absolute value of the positive radial distance is greater than the negative radial distance, the preform can be made and the optical fibre can be drawn.

## 4. Conclusion

A negative curvature tube ARF is designed for the transmission of OAM modes. The structure can stably support the transmission of 30 OAM modes in the range of 1.50–1.60 $\mu$m. The simulation results show that the refractive index difference of the ARF is greater than $1 \times 10^{-4}$ without additional doping and there is no mode degeneracy. The structure has low and flat dispersion characteristics such as dispersion variation of only 5.98 ps/(km nm) and the confinement loss at 1.55 μm is very low ranging from $10^{-9}$ to $10^{-11}$ dB/m. The optical fibre also has a small nonlinear coefficient as low as 0.539 $\text{km}^{-1}\,\text{W}^{-1}$ at 1.55 μm boding well for OAM mode transmission. The mode purity of all the OAM modes is more than 98.295% and the ARF can be manufactured by the fibre stack technique. The excellent properties render the structure desirable in optical communication.

**Table 2.** Comparison of the minimum confinement loss.

| This paper | Ref. [9] | Ref. [31] | Ref. [32] | Ref. [33] |
|---|---|---|---|---|
| $10^{-11}$to $10^{-9}$ dB/m | $10^{-9}$to $10^{-3}$ dB/m | $10^{-9}$ dB/m | $10^{-9}$to $10^{-4}$ dB/m | $10^{-10}$to $10^{-4}$ dB/m |

## Funding

This work was jointly supported by the Local Universities Reformation and Development Personnel Training Supporting Project from Central Authorities [140119001], City University of Hong Kong Strategic Research Grant (SRG) [grant number 7005505], and Scientific Research Fund of Sichuan Province Science and Technology Department [2020YJ0137].

## References

[1] Li S, Wang J. A compact trench-assisted multi-orbital-angular-momentum multi-ring fiber for ultrahigh-density space-division multiplexing (19 rings × 22 modes). Sci Rep. 2014;4(1). doi:10.1038/srep03853.
[2] Zhu B, et al. 112-Tb/s space-division multiplexed DWDM transmission with 14-b/s/Hz aggregate spectral efficiency over a 76.8-km seven-core fiber. Opt Express. 2011;19(17). doi:10.1364/OE.19.016665.
[3] Koji I, et al. Ultra-dense spatial-division-multiplexed optical fiber transmission over 6-mode 19-core fibers. Opt Express. 2016;24(10). doi:10.1364/OE. 24.010 213.
[4] Shuhui L, Jian W. Supermode fiber for orbital angular momentum (OAM) transmission. Opt Express. 2015; 23(14). doi:10.1364/OE.23.018736.
[5] McMorran Benjamin J, et al. Origins and demonstrations of electrons with orbital angular momentum. Philos Trans A Math Phys Eng Sci. 2017;375(2087). doi:10.1098/rsta.2015.0434.
[6] Kibler B, et al. Octave-spanning coherent supercontinuum generation in a step-index tellurite fiber and towards few-cycle pulse compression at 2 [formula omitted]. Opt Commun. 2021;488. doi:10.1016/J.OPTCOM.2021.126853.
[7] Majumdar A, et al. A simple method for prediction of effective core area and index of refraction of single-mode graded index fiber in the Low V region. J Opt Commun. 2014;35(4). doi:10.1515/joc-2014-0020.
[8] Israk M. F. . Ring-based coil structure photonic crystal fiber for transmission of Orbital Angular Momentum with large bandwidth: Outline, investigation and analysis . Optics Communications. 2020;473:126003.
[9] Tian W, et al. A circular photonic crystal fiber supporting 26 OAM modes. Optical Fiber Technology. 2016;30. doi:10.1016/j.yofte.2016.07.009.
[10] Brunet C, Rusch LA. Optical fibers for the transmission of orbital angular momentum modes. Optical Fiber Technology. 2017;35. doi:10.1016/j.yofte.2016.09.016.
[11] Shou-Fei G, et al. "Nodeless hollow-core fiber for the visible spectral range. Opt Lett. 2017;42(1). doi:10.1364/OL.42.000061.
[12] Couny F, Benabid F, Light PS. Large-pitch kagome-structured hollow-core photonic crystal fiber. Opt Lett. 2006;31(24):3574–3576.
[13] Debord B, et al. Ultra-large core size hypocycloid-shape inhibited coupling Kagome fibers for high-energy laser beam handling. J Lightwave Technol. 2015;33(17): 3630–3634.
[14] Kosolapov AF, et al. Hollow-core revolver fibre with a double-capillary reflective cladding. Quantum Elec (Woodbury). 2016;46(3). doi:10.1070/QEL15972.
[15] Chaudhuri S, et al. Low Lo SS transmission in negative curvature optical fibers with elliptical capillary tubes. J Lightwave Technol. 2016;34(18):4228–4231.
[16] Hayes JR, et al. Antiresonant hollow core fiber with an octave spanning bandwidth for short haul data communications. J Lightwave Technol. 2017;35(3):437–442.
[17] Xiang C, et al. Double negative curvature anti-resonance hollow core fiber. Opt Express. 2019;27(14). doi:10.1364/OE.27.019548.
[18] Liu C, et al. "Design and theoretical analysis of a photonic crystal fiber based on surface plasmon resonance sensing.". J Nanophotonics. 2015;9(1). doi:10.1117/1.JNP.9.093050.
[19] Hisatomi M, Parker MC, Walker SD. Singular optical fibre featuring refractive index dislocation for chiral waveguiding of high orbital angular momentum light. IEEE. 2005;CWAB3-P80:959–960.
[20] Xiuli B, et al. A new type bragg fiber for supporting 50 orbital angular momentum modes. Optik (Stuttg). 2020;219; doi:10.1016/J.IJLEO.2020.165153.
[21] Cao Y, et al. Highly birefringent photonic crystal fibers with flattened dispersion and low confinement loss. Optoelectron Lett. 2013;9(1). doi:10.1007/s11801-013-2336-8.
[22] Anowar Kabir M, et al. Design and performance evaluation of photonic crystal fibers of supporting orbital angular momentum states in optical transmission. Opt Commun. 2020;467. doi:10.1016/j.optcom.2020.125731.
[23] Ahmad A-ZF, Kawsar A. Novel design of dual guided photonic crystal fiber for large capacity transmission in high-speed optics communications with supporting good quality OAM and LP modes. Alexandria Eng J. 2020;59(6). doi:10.1016/J.AEJ.2020.09.004.
[24] Anowar Kabir M, et al. Novel spider web photonic crystal fiber for robust mode transmission applications with supporting orbital angular momentum transmission property. Opt Quantum Electron. 2020;52(4). doi:10.1007/s11082-020-02447-w.
[25] He T, et al. Low confinement loss photonic crystal fibre capable of supporting 54 orbital angular momentum modes. Journal of Modern Optics. 2020;67(6).
[26] Wan X, et al. Low dispersion and confinement loss photonic crystal fiber for orbital angular momentum mode transmission. Opt Quantum Electron. 2020;52(6). doi:10.1007/s11082-020-02414-5.
[27] Zhang L, et al. Circular photonic crystal fiber supporting 110 OAM modes. Opt Commun. 2018;429; doi:10.1016/j.optcom.2018.07.014.
[28] Yang Y, et al. Octave-spanning supercontinuum generation of vortices in an As2S3 ring photonic crystal fiber. Opt Lett. 2012;37(11). doi:10.1364/OL.37.001889.
[29] Bai X, et al. Design of a circular photonic crystal fiber with square air-holes for orbital angular momentum modes transmission. Optik (Stuttg). 2018;158; doi:10.1016/j.ijleo.2018.01.015.
[30] Lei Y, et al. Numerical analysis of a photonic crystal fiber for supporting 76 orbital angular momentum modes. J Opt. 2018;20(10). doi:10.1088/2040-8986/aaddb8.

[31] Xun X, et al. Theoretical proposal of a low-loss wide-bandwidth silicon photonic crystal fiber for supporting 30 orbital angular momentum modes. PloS one. 2017;12(12). doi:10.1371/journal.pone.0189660.
[32] A design strategy of the circular photonic crystal fiber supporting good quality orbital angular momentum mode transmission. Opt Commun 2017;397: 59–66.
[33] Hu Z, et al. A New type circular photonic crystal fiber for orbital angular momentum mode transmission. IEEE Photonics Technol Lett. 2016;28(13):1426–1429.